Editors' Suggestion

Macroscopic quantum electrodynamics theory of resonance energy transfer involving chiral molecules

Janine Christine Franz*
Physikalisches Institut, Albert-Ludwigs-Universität Freiburg, Hermann-Herder-Straße 3, 79104 Freiburg, Germany

Stefan Yoshi Buhmann†
Institut für Physik, Universität Kassel, Heinrich-Plett-Straße 40, 34132 Kassel, Germany

A. Salam‡
Department of Chemistry, Wake Forest University, Winston-Salem, North Carolina 27109, USA

(Received 30 September 2022; accepted 21 February 2023; published 10 March 2023)

Resonance energy transfer between chiral molecules can be used to discriminate between different enantiomers. The transfer rate between chiral molecules consists of nondiscriminatory and discriminatory parts. We derive these two rate contributions in the framework of macroscopic quantum electrodynamics. We show that their ratio is usually larger in the retarded regime or far zone of large separation distances and that the degree of discrimination can be modified when considering a surrounding medium. We highlight the importance of local field effects onto the degree of discrimination and predict for general identical chiral molecules the optimum dielectric medium for discrimination. We apply our results to 3-methylcyclopentanone and show that exotic media can even invert the discriminatory effect.

DOI: 10.1103/PhysRevA.107.032809

I. INTRODUCTION

A key feature of macroscopic quantum electrodynamics (QED) [1,2] that proves advantageous when it is deployed is that it is able to treat objects that are large relative to the atomic scale such as plates, slabs, and other geometrical bodies. Another benefit is that it also accounts for the presence of an environment. The surroundings, for example, may be taken to be purely electric or magnetic, or a combination of the two as in a magnetodielectric medium, or even be chiral. Noteworthy successful early applications of the formalism included the calculation of Casimir–van der Waals forces [3–5]. Recently, a number of other problems that require the use of the quantum properties of light have been tackled. Some of these have covered the generation of hybrid light-matter (polaritonic) states via ultrastrong coupling, including those due to the presence of a cavity, and its influence on chemical reactivity [6–12], the simulation of molecular emission power spectra [13–15], modeling Auger decay and interatomic Coulombic decay [16–21], as well as predicting discriminatory optical forces occurring between chiral systems [22–28]. Another important interparticle process that has been considered, and which is of wide-ranging scientific and technological interest, is resonance energy transfer (RET) [29,30], in what was an early application in chemical physics of the polariton concept [31,32]. Subsequent effort has explored the role of a third body in mediating migration of energy in a dielectric medium, the different pathways that may ensue, and the interesting coherence and decoherence effects this gives rise to [33–35]. This has extended a large body of work (see the references cited in a couple of recent reviews [36,37]) in which the RET phenomenon has been evaluated and fully understood using molecular QED theory [38–41], where in contrast to macroscopic QED, the Maxwell fields propagate and are quantized in free space instead of in a medium. Conveyance of electronic energy takes place via the exchange of a single virtual photon [42] between emitter and absorber species, and the rate is computed perturbatively using the Fermi golden rule.

A novel feature emerges on relaxing the common electric dipole approximation. Including the magnetic dipole coupling term enables a discriminatory contribution to the pair transfer rate to occur which applies to migration of energy between two chiral molecules [43,44]. Replacing one of the enantiomers of the pair by its antipodal form changes the sign of the discriminatory contribution. This makes RET a candidate for the development of a new chiral discrimination technique. While chiral molecules possess similar to identical physico-chemical properties, such as boiling and melting points, solubility, and absorption spectra, they can have very different biological properties especially when interacting with other chiral objects. In particular, for chiral drugs, the different enantiomers may have very different effects on the human body. As roughly 56% of all drugs in the pharmaceutical industry are made up of chiral molecules, measuring and controlling the excess of one enantiomer in a mixture of chiral molecules is a key aim [45].

*janine.franz@physik.uni-freiburg.de
†stefan.buhmann@uni-kassel.de
‡salama@wfu.edu

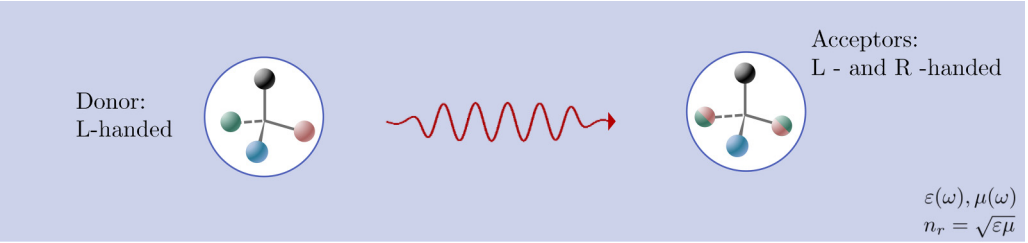

FIG. 1. Scheme of the considered setup: Two chiral molecules, one excited (donor) and one in its ground state (acceptor), undergo resonance energy transfer. The donor's handedness is assumed to be known while the acceptor's handedness could be either left or right. We place the system inside a medium and take local field effects and screening corrections around the donor and the acceptor into account.

In this work we employ the formalism of macroscopic QED to calculate the RET rate between a chiral donor and a chiral acceptor in a magnetoelectric medium. On choosing conditions appropriate to a vacuum electromagnetic field, previous free-space QED results are recovered. Screening corrections and local field effects are taken into account by utilizing a real cavity model to treat the influence of a surrounding medium, extending electric dipole-dipole transfer in a dielectric medium [32] to the important case of chiral molecules exchanging energy in a complex environment. Interestingly, it is found that the discriminatory rate may be enhanced in a magnetoelectric medium. Conditions when this occurs are investigated. The theory developed is applied to the chiral molecule 3-methylcyclopentanone (3MCP). After a brief presentation of the macroscopic QED formalism tailored to the RET problem, the transition matrix element and rate for transfer between two optically active molecules in a magneto-electric medium are derived in Sec. II. The free-space discriminatory rate is obtained and the degree of discrimination is quantified in Sec. III. In Sec. IV, we investigate the variation of the degree of discrimination as a function of separation distance and differing medium characteristics to model a number of different solvents. Conclusions are briefly given in Sec. V.

II. RESONANCE ENERGY TRANSFER RATE

We derive, within the framework of macroscopic QED, the resonance energy transfer rate between a chiral donor molecule, D, and a chiral acceptor, A, in a medium (see Fig. 1). In QED parlance, RET arises from the exchange of a single virtual photon (or polariton in the case of exchange occurring in a medium) between the two particles [36]. The total Hamiltonian operator for the system, in which D is initially excited in the state $|1\rangle_{\rm D}$ and A is in its ground state $|0\rangle_{\rm A}$, is given by

$$\hat{H} = \hat{H}_{\rm D} + \hat{H}_{\rm A} + \hat{H}_{\rm F} + \hat{H}_{\rm ia}, \tag{1}$$

where $\hat{H}_{\rm D/A}$ is the particle Hamiltonian for D/A, $\hat{H}_{\rm F}$ is the radiation field Hamiltonian, and the last term denotes the interaction Hamiltonian for the coupling of the electromagnetic field to each molecule. Because we assume each species to be optically active, the magnetic and the usual electric dipoles couple to the magnetic field $\hat{\boldsymbol{B}}$ and the electric field $\hat{\boldsymbol{E}}$ as

$$\hat{H}_{\rm ia} = -\sum_{\alpha={\rm D,A}} [\hat{\boldsymbol{d}}^{(\alpha)} \cdot \hat{\boldsymbol{E}}(\boldsymbol{r}_\alpha) + \hat{\boldsymbol{m}}^{(\alpha)} \cdot \hat{\boldsymbol{B}}(\boldsymbol{r}_\alpha)], \tag{2}$$

where $\boldsymbol{r}_{\rm D/A}$ is the donor's or the acceptor's position, $\hat{\boldsymbol{d}}^{\rm D/A}$ is the donor's or the acceptor's electric dipole moment operator, and $\hat{\boldsymbol{m}}^{\rm D/A}$ is its magnetic counterpart. The energy migration rate Γ is calculated using Fermi's golden rule,

$$\Gamma = \frac{2\pi}{\hbar^2}\rho(\omega_f)|M_{\rm fi}|^2, \tag{3}$$

where $M_{\rm fi}$ is the matrix element for the transition between the initial and the final state, and $\rho(\omega_f)$ is the density of final states with energy $E_f = \hbar\omega_f$. To leading order, $M_{\rm fi}$ is evaluated from the second-order perturbation theory formula

$$M_{\rm fi} = \sum_j \frac{\langle f|\hat{H}_{\rm ia}|j\rangle\,\langle j|\hat{H}_{\rm ia}|i\rangle}{E_i - E_j}\Big|_{E_i=E_f}, \tag{4}$$

where E_x is the energy of the respective state $|x\rangle$ and for the system of interest the initial and final states are given by $|i\rangle = |1\rangle_{\rm D}|0\rangle_{\rm A}|\{0\}\rangle_F$ and $|f\rangle = |0\rangle_{\rm D}|1\rangle_{\rm A}|\{0\}\rangle_F$. Our analysis focuses on only one donor and acceptor pair. The extension to N particles is, however, straightforward. By summing over all possible final states one can account for n ground-state acceptors and m excited donors. Only if multiple donors share an excitation does the calculation become more involved and superradiance effects occur [46].

From Eq. (4), it is necessary to sum over all possible intermediate states

$$|j\rangle \in \{|j_1(\sigma,\omega,\boldsymbol{r})\rangle\,, |j_2(\sigma,\omega,\boldsymbol{r})\rangle\,;\, \forall\sigma,\boldsymbol{r},\omega\}, \tag{5}$$

with

$$|j_1(\sigma,\omega,\boldsymbol{r})\rangle = |0\rangle_{\rm D}|0\rangle_{\rm A}|\mathbf{1}_\sigma(\omega,\boldsymbol{r})\rangle_F\,, \tag{6}$$

$$|j_2(\sigma,\omega,\boldsymbol{r})\rangle = |1\rangle_{\rm D}|1\rangle_{\rm A}|\mathbf{1}_\sigma(\omega,\boldsymbol{r})\rangle_F\,, \tag{7}$$

where $|0/1\rangle_{\rm D/A}$ is the ground or excited state of the donor or acceptor molecule and $|\mathbf{1}_\sigma(\omega,\boldsymbol{r})\rangle_F = \hat{\boldsymbol{f}}^\dagger_\sigma(\boldsymbol{r},\omega)|\{0\}\rangle_F$ is the single-quantum Fock state of collective, polaritonlike bosonic excitations of electric and magnetic types ($\sigma = {\rm e/m}$) at position $\boldsymbol{r}$ with energy $\hbar\omega$. The creation and annihilation operators $\hat{\boldsymbol{f}}^\dagger_\sigma(\boldsymbol{r},\omega)$ and $\hat{\boldsymbol{f}}_\sigma(\boldsymbol{r},\omega)$ fulfill the commutation relations

$$[\hat{\boldsymbol{f}}_\sigma(\boldsymbol{r},\omega), \hat{\boldsymbol{f}}^\dagger_{\sigma'}(\boldsymbol{r}',\omega')] = \delta_{\sigma\sigma'}\boldsymbol{\delta}(\boldsymbol{r}-\boldsymbol{r}')\delta(\omega-\omega') \tag{8}$$

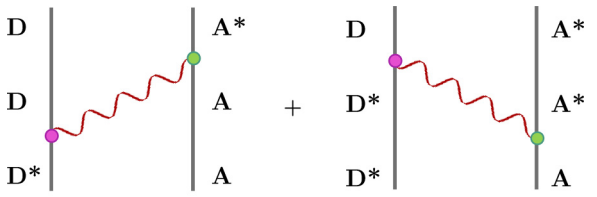

FIG. 2. Feynman diagrams for RET between chiral particles: Each intersection between a wavy line and a solid line represents a particle-field interaction. Each interaction can either be electric or magnetic. The two diagrams result in different frequency poles [see Eq. (18)].

and may be used to expand the electric and magnetic fields as

$$\hat{\boldsymbol{E}}(\boldsymbol{r}) = \int_0^\infty d\omega \hat{\boldsymbol{E}}(\boldsymbol{r},\omega) + \text{H.c.}, \tag{9}$$

$$\hat{\boldsymbol{E}}(\boldsymbol{r},\omega) = \sum_{\sigma=\text{e,m}} \int d^3r' \mathbb{G}_\sigma(\boldsymbol{r},\boldsymbol{r}',\omega)\cdot\hat{\boldsymbol{f}}_\sigma(\boldsymbol{r}',\omega), \tag{10}$$

$$\hat{\boldsymbol{B}}(\boldsymbol{r}) = \int_0^\infty d\omega \hat{\boldsymbol{B}}(\boldsymbol{r},\omega) + \text{H.c.}, \tag{11}$$

$$\hat{\boldsymbol{B}}(\boldsymbol{r},\omega) = \frac{1}{i\omega}\sum_{\sigma=\text{e,m}} \int d^3r' \overrightarrow{\nabla}\times\mathbb{G}_\sigma(\boldsymbol{r},\boldsymbol{r}',\omega)\cdot\hat{\boldsymbol{f}}_\sigma(\boldsymbol{r}',\omega). \tag{12}$$

The Green's tensor $\mathbb{G}_\sigma$ is defined via the Helmholtz equation and is given explicitly in Appendix A. The RET process may be visualized by the two Feynman diagrams of Fig. 2. They reflect the two possible propagation directions associated with single virtual photon-polariton exchange between emitter and absorber. Each intersection of a solid line with a wavy line represents an interaction between the respective particle and the field. Based on the coupling Hamiltonian, Eq. (2), electric $(-\hat{\boldsymbol{d}}\cdot\hat{\boldsymbol{E}})$ as well as magnetic $(-\hat{\boldsymbol{m}}\cdot\hat{\boldsymbol{B}})$ dipole interactions with the Maxwell field operators have to be considered. The probability amplitude can therefore be divided into four terms,

$$M_{\text{fi}} = M_{\text{ee}} + M_{\text{em}} + M_{\text{me}} + M_{\text{mm}}, \tag{13}$$

where the first and second subscripts imply electric or magnetic interaction of A and D with the field, respectively. By using the vacuum correlation functions of the electromagnetic fields (see Appendix B),

$$\langle\hat{\boldsymbol{E}}(\boldsymbol{r}_\text{D},\omega)\otimes\hat{\boldsymbol{E}}^\dagger(\boldsymbol{r}_\text{A},\omega')\rangle_\text{vac} = \frac{\hbar\mu_0\omega^2}{\pi}\delta(\omega-\omega')\text{Im}\mathbb{G}\times(r_\text{A},r_\text{D},\omega), \tag{14}$$

$$\langle\hat{\boldsymbol{E}}(\boldsymbol{r}_\text{D},\omega)\otimes\hat{\boldsymbol{B}}^\dagger(\boldsymbol{r}_\text{A},\omega')\rangle_\text{vac} = -\frac{i\hbar\mu_0\omega}{\pi}\delta(\omega-\omega')\text{Im}\mathbb{G}(r_\text{A},r_\text{D},\omega)\times\overleftarrow{\nabla}_\text{D}, \tag{15}$$

$$\langle\hat{\boldsymbol{B}}(\boldsymbol{r}_\text{D},\omega)\otimes\hat{\boldsymbol{E}}^\dagger(\boldsymbol{r}_\text{A},\omega')\rangle_\text{vac} = -i\frac{\hbar\mu_0\omega}{\pi}\delta(\omega-\omega')\overrightarrow{\nabla}_\text{A}\times\text{Im}\mathbb{G}(r_\text{A},r_\text{D},\omega), \tag{16}$$

$$\langle\hat{\boldsymbol{B}}(\boldsymbol{r}_\text{D},\omega)\otimes\hat{\boldsymbol{B}}^\dagger(\boldsymbol{r}_\text{A},\omega')\rangle_\text{vac} = -\frac{\hbar\mu_0}{\pi}\delta(\omega-\omega')\overrightarrow{\nabla}_\text{A}\times\text{Im}\mathbb{G}(r_\text{A},r_\text{D},\omega)\times\overleftarrow{\nabla}_\text{D}, \tag{17}$$

we can derive the transition matrix elements in terms of the Green's tensor for general environments, with that for the second term of Eq. (13) given as (see Appendix B)

$$\begin{aligned} M_\text{em} &= -\frac{1}{\hbar}\int d\omega\left\{\frac{1}{\omega-\omega_\text{D}}\boldsymbol{d}^\text{A}\cdot\langle\hat{\boldsymbol{E}}_\text{A}\otimes\hat{\boldsymbol{B}}_\text{D}^{\prime\dagger}\rangle_\text{vac}\cdot\boldsymbol{m}^\text{D}\right. \\ &\quad\left.+\frac{1}{\omega+\omega_\text{A}}\boldsymbol{m}^\text{D}\cdot\langle\hat{\boldsymbol{B}}_\text{D}\otimes\hat{\boldsymbol{E}}_\text{A}^{\prime\dagger}\rangle_\text{vac}\cdot\boldsymbol{d}^\text{A}\right\} \\ &= \frac{\mu_0c^2}{\pi}\int d\omega\left\{\frac{1}{\omega-\omega_\text{D}}+\frac{1}{\omega+\omega_\text{D}}\right\} \\ &\quad\times\boldsymbol{d}^\text{A}\cdot\text{Im}\mathbb{G}(r_\text{A},r_\text{D},\omega)\times\overleftarrow{\nabla}_\text{D}\cdot\boldsymbol{m}^\text{D}, \end{aligned} \tag{18}$$

where $\omega_\text{D} = \omega_1^\text{D} - \omega_0^\text{D}$ is the transition frequency of the donor and the acceptor's transition frequency is $\omega_\text{A} = \omega_1^\text{A} - \omega_0^\text{A} = \omega_\text{D}$ from energy conservation, and we introduced the shorthand-notation $\hat{\boldsymbol{E}}_\text{A/D} = \hat{\boldsymbol{E}}(\boldsymbol{r}_\text{A/D},\omega)$, analogously for $\hat{\boldsymbol{B}}$, while the prime indicates the substitution of $\omega\to\omega'$ and the arrows on the ∇ operator denote the direction which the derivative acts on. Additionally, we introduced the following notation for the downward and upward dipolar transitions in D and A, respectively: $\boldsymbol{d}^\text{D} = \langle 0|\hat{\boldsymbol{d}}|1\rangle_\text{D}$ and $\boldsymbol{d}^\text{A} = \langle 1|\hat{\boldsymbol{d}}|0\rangle_\text{A}$, with analogous definitions for $\boldsymbol{m}^\text{D/A}$. The remaining transition matrix elements can be derived similarly and the pole integration can be calculated generally as

$$\begin{aligned} &\int d\omega\left\{\frac{f(\omega)}{\omega-\omega_\text{D}}+\frac{f(-\omega)}{\omega+\omega_\text{A}}\right\}\text{Im}\mathbb{G}(\omega) \\ &\quad\longrightarrow\lim_{\epsilon\to0^+}\int d\omega\left\{\frac{f(\omega)}{\omega-(\omega_\text{D}+i\epsilon)}+\frac{f(-\omega)}{\omega+\omega_\text{A}}\right\} \\ &\quad\times\frac{1}{2i}[\mathbb{G}(\omega)+\mathbb{G}(-\omega)] \\ &\quad=\pi f(\omega_\text{D})\mathbb{G}(\omega_\text{D}), \end{aligned} \tag{19}$$

for $\omega_\text{A} = \omega_\text{D}$ and $f(\omega) = \omega^n$ with $n\in\{0,1,2\}$. The correct regularization of the pole on the real axis follows from revisiting the derivation of Fermi's golden rule, and the detailed pole integration is given in Appendix C. This finally yields the desired transition matrix elements

$$M_\text{ee} = -\mu_0\omega_\text{D}^2\boldsymbol{d}^\text{A}\cdot\mathbb{G}(\boldsymbol{r}_\text{A},\boldsymbol{r}_\text{D},\omega_\text{D})\cdot\boldsymbol{d}^\text{D}, \tag{20a}$$

$$M_\text{em} = i\mu_0\omega_\text{D}\boldsymbol{d}^\text{A}\cdot\mathbb{G}(\boldsymbol{r}_\text{A},\boldsymbol{r}_\text{D},\omega_\text{D})\times\overleftarrow{\nabla}_\text{D}\cdot\boldsymbol{m}^\text{D}, \tag{20b}$$

$$M_\text{me} = i\mu_0\omega_\text{D}\boldsymbol{m}^\text{A}\cdot\overrightarrow{\nabla}_\text{A}\times\mathbb{G}(\boldsymbol{r}_\text{A},\boldsymbol{r}_\text{D},\omega_\text{D})\cdot\boldsymbol{d}^\text{D}, \tag{20c}$$

$$M_\text{mm} = \mu_0\boldsymbol{m}^\text{A}\cdot\overrightarrow{\nabla}_\text{A}\times\mathbb{G}(\boldsymbol{r}_\text{A},\boldsymbol{r}_\text{D},\omega_\text{D})\times\overleftarrow{\nabla}_\text{D}\cdot\boldsymbol{m}^\text{D}. \tag{20d}$$

One can easily verify that they lead to the same results known from free-space QED [43]. In vacuum, the Green's tensor is given by (see Appendix A)

$$\mathbb{G}^{(0)}(\boldsymbol{r}_\text{A},\boldsymbol{r}_\text{D},\omega) = \left[\mathbb{I}+\frac{\nabla\nabla}{k^2}\right]\frac{e^{ikr}}{4\pi r}, \tag{21}$$

with $r = |\boldsymbol{r}_\mathrm{D} - \boldsymbol{r}_\mathrm{A}|$, $k = \omega/c$, $\mathbb{I}$ being the 3×3-identity matrix, $\nabla = \overrightarrow{\nabla}$, and $\nabla\nabla = \nabla \otimes \nabla$. For dipoles of the same type at each particle, familiar matrix elements ensue [39],

$$M_\mathrm{ee} = -\mu_0 c^2 d_i^\mathrm{A}[k^2\delta_{ij} + \nabla_i\nabla_j]\frac{e^{ikr}}{4\pi r}d_j^\mathrm{D} = \frac{1}{4\pi\varepsilon_0}d_i^\mathrm{A}d_j^\mathrm{D}[\nabla^2\delta_{ij} - \nabla_i\nabla_j]\frac{e^{ikr}}{r}, \tag{22}$$

$$M_\mathrm{mm} = \mu_0 m_i^\mathrm{A}\left[-\nabla\times\mathbb{I}\times\nabla + \nabla\times\frac{\nabla\nabla}{k^2}\times\nabla\right]_{ij}\frac{e^{ikr}}{4\pi r}m_j^\mathrm{D} = -\mu_0 m_i^\mathrm{A}m_j^\mathrm{D}[\nabla\times\mathbb{I}\times\nabla]_{ij}\frac{e^{ikr}}{4\pi r} = \frac{1}{4\pi\varepsilon_0 c^2}m_i^\mathrm{A}m_j^\mathrm{D}[\nabla^2\delta_{ij} - \nabla_i\nabla_j]\frac{e^{ikr}}{r}, \tag{23}$$

while for the mixed dipole term, crucial for transfer between chiral systems [43],

$$M_\mathrm{em} + M_\mathrm{me} = \frac{ik}{4\pi\varepsilon_0 c}\left(d_i^\mathrm{D}m_j^\mathrm{A} - m_i^\mathrm{D}d_j^\mathrm{A}\right)\epsilon_{ijk}\nabla_k\frac{e^{ikr}}{r}, \tag{24}$$

where we used

$$[\overrightarrow{\nabla}_\mathrm{A}\times\mathbb{G}(r_\mathrm{A}, r_\mathrm{D}, \omega)]_{ij} = -\epsilon_{ijk}\nabla_k\frac{e^{ikr}}{4\pi r} = -[\mathbb{G}(r_\mathrm{A}, r_\mathrm{D}, \omega)\times\overleftarrow{\nabla}_\mathrm{A}]_{ij}. \tag{25}$$

Inserting the matrix elements in terms of the general Green's tensor (20a)–(20d) into Fermi's golden rule (3) leads to the rate for a general environment:

$$\Gamma = \sum_{\lambda_1,\lambda_2,\lambda_3,\lambda_4}\Gamma_{\lambda_1\lambda_2\lambda_3\lambda_4}, \tag{26}$$

$$\Gamma_{\lambda_1\lambda_2\lambda_3\lambda_4} = \frac{2\pi\rho\mu_0^2}{9\hbar^2}\left(\boldsymbol{d}_{\lambda_1}^\mathrm{A}\cdot\boldsymbol{d}_{\lambda_2}^{\mathrm{A}*}\right)\left(\boldsymbol{d}_{\lambda_3}^{\mathrm{D}*}\cdot\boldsymbol{d}_{\lambda_4}^\mathrm{D}\right) \times \mathrm{Tr}\left[\mathbb{G}_{\lambda_1\lambda_4}\cdot\mathbb{G}_{\lambda_2\lambda_3}^{*T}\right], \tag{27}$$

where we have assumed that the transitions are isotropic, such that $\boldsymbol{d}_1 \otimes \boldsymbol{d}_2 = (\boldsymbol{d}_1\cdot\boldsymbol{d}_2)\mathbb{I}/3$ and we adopted a dual formulation with $\lambda_i \in \{\mathrm{e}, \mathrm{m}\}$. The rate depends on the absolute square of the transition matrix element and involves hence the interference of all possible process channels (see Fig. 2). In the dual rate contributions (27), $\lambda_{1/2}$ label the type of interactions of the acceptor with the field and $\lambda_{3/4}$ the ones of the donor. The relevant dual quantities are

$$\boldsymbol{d}_\mathrm{e} = \boldsymbol{d}, \qquad \boldsymbol{d}_\mathrm{m} = \frac{\boldsymbol{m}}{c}, \tag{28a}$$

$$\mathbb{G}_\mathrm{ee} = \frac{i\omega}{c}\mathbb{G}(\boldsymbol{r}_\mathrm{A}, \boldsymbol{r}_\mathrm{D}, \omega)\frac{i\omega}{c}, \tag{28b}$$

$$\mathbb{G}_\mathrm{mm} = \overrightarrow{\nabla}_\mathrm{A}\times\mathbb{G}(\boldsymbol{r}_\mathrm{A}, \boldsymbol{r}_\mathrm{D}, \omega)\times\overleftarrow{\nabla}_\mathrm{D}, \tag{28c}$$

$$\mathbb{G}_\mathrm{em} = \frac{i\omega}{c}\mathbb{G}(\boldsymbol{r}_\mathrm{A}, \boldsymbol{r}_\mathrm{D}, \omega)\times\overleftarrow{\nabla}_\mathrm{D}, \tag{28d}$$

$$\mathbb{G}_\mathrm{me} = \overrightarrow{\nabla}_\mathrm{A}\times\mathbb{G}(\boldsymbol{r}_\mathrm{A}, \boldsymbol{r}_\mathrm{D}, \omega)\frac{i\omega}{c}, \tag{28e}$$

where $\hbar\omega = \hbar\omega^\mathrm{D} = \hbar\omega^\mathrm{A}$ is the transition energy. When the handedness of one participating molecule is known, the rate can be used to discriminate between different enantiomers of the second entity. Without loss of generality, we take the donor to be left-handed while the acceptor species may be of either handedness (see Fig. 1). Molecular chirality may be characterized by the scalar product between magnetic and electric transition dipole moments, which is related to the rotatory strength R of the respective chiral molecule through

$$\frac{R}{c} = \mathrm{Im}[\langle 0|\hat{\boldsymbol{d}}_\mathrm{e}|1\rangle\cdot\langle 1|\hat{\boldsymbol{d}}_\mathrm{m}|0\rangle], \tag{29}$$

and whose sign depends on the molecule's handedness. In our notational convention, where $\boldsymbol{d}_\lambda^\mathrm{D}$ denotes a downward transition, while $\boldsymbol{d}_\lambda^\mathrm{A}$ represents an upward transition, the respective rotatory strengths of D and A are given by

$$\frac{R^\mathrm{D}}{c} = \mathrm{Im}\left[\boldsymbol{d}_\mathrm{e}^\mathrm{D}\cdot\boldsymbol{d}_\mathrm{m}^{\mathrm{D}*}\right] = -i\boldsymbol{d}_\mathrm{e}^\mathrm{D}\cdot\boldsymbol{d}_\mathrm{m}^{\mathrm{D}*} = i\boldsymbol{d}_\mathrm{e}^{\mathrm{D}*}\cdot\boldsymbol{d}_\mathrm{m}^\mathrm{D}, \tag{30}$$

$$\frac{R^\mathrm{A}}{c} = \mathrm{Im}\left[\boldsymbol{d}_\mathrm{e}^{\mathrm{A}*}\cdot\boldsymbol{d}_\mathrm{m}^\mathrm{A}\right] = i\boldsymbol{d}_\mathrm{e}^\mathrm{A}\cdot\boldsymbol{d}_\mathrm{m}^{\mathrm{A}*} = -i\boldsymbol{d}_\mathrm{e}^{\mathrm{A}*}\cdot\boldsymbol{d}_\mathrm{m}^\mathrm{A}, \tag{31}$$

where we have explicitly assumed real electric transition dipole moments $\boldsymbol{d}_\mathrm{e} = \boldsymbol{d}_\mathrm{e}^*$ and imaginary magnetic dipole moments $\boldsymbol{d}_\mathrm{m} = -\boldsymbol{d}_\mathrm{m}^*$.

III. DISCRIMINATION IN FREE SPACE

With these preparations at hand, we can partition the rate into different contributions, depending on their sensitivity to the acceptor's handedness. The potentially discriminatory contributions that are proportional to the acceptor's optical rotatory strength R^A are

$$\Gamma_\mathrm{disc} = \sum_{\lambda_1\lambda_2}(\Gamma_{\mathrm{em}\lambda_1\lambda_2} + \Gamma_{\mathrm{me}\lambda_1\lambda_2}), \tag{32}$$

where $\lambda_1, \lambda_2 \in \{\mathrm{e}, \mathrm{m}\}$ label electric and magnetic interactions of the donor. These rate contributions are of two different forms:

$$\Gamma_{\mathrm{em}\lambda\lambda} \propto R^\mathrm{A}\left|\boldsymbol{d}_\lambda^\mathrm{D}\right|^2\mathrm{Tr}\left[\mathbb{G}_{\mathrm{e}\lambda}\cdot\mathbb{G}_{\mathrm{m}\lambda}^{*T}\right], \tag{33}$$

$$\Gamma_{\mathrm{em}\lambda_1\lambda_2} \propto R^\mathrm{A}R^\mathrm{D}\,\mathrm{Tr}\left[\mathbb{G}_{\mathrm{e}\lambda_1}\cdot\mathbb{G}_{\mathrm{m}\lambda_2}^{*T}\right], \tag{34}$$

with $\lambda_1 \neq \lambda_2$ and analogously for $\Gamma_{\mathrm{me}\lambda_1\lambda_2}$. The rotatory strength $R_\mathrm{A/D} \propto \boldsymbol{d}\cdot\boldsymbol{m}$ is a chiral property in the sense that its sign changes depending on the molecule's handedness. On the other hand, the absolute square of the magnetic or electric dipole is not sensitive to the handedness. In agreement with Curie's dissymmetry principle, contributions of the first kind [Eq. (33)] vanish in free space: $\mathrm{Tr}[\mathbb{G}_{e\lambda}\cdot\mathbb{G}_{m\lambda}^{*T}] = \mathrm{Tr}[\mathbb{G}_{m\lambda}\cdot\mathbb{G}_{e\lambda}^{*T}] = 0$, $\forall\lambda$. Only contributions that emerge from the chiral properties of both the donor and the acceptor, i.e., that are proportional to the product $R_\mathrm{A}R_\mathrm{D}$, can discriminate the acceptor's enantiomers. We are hence left with the discriminatory rate contribution in free space,

$$\Gamma_\mathrm{disc} = \Gamma_\mathrm{emme} + \Gamma_\mathrm{meme} + \Gamma_\mathrm{emem} + \Gamma_\mathrm{meem}, \tag{35}$$

and the nondiscriminatory rate contribution,

$$\Gamma_\mathrm{nd} = \sum_{\lambda_1\lambda_2}\Gamma_{\lambda_1\lambda_1\lambda_2\lambda_2}, \tag{36}$$

which yield the total rate for left(L)- and right(R)-handed acceptors, $\Gamma_\mathrm{L/R} = \Gamma_\mathrm{nd} \pm |\Gamma_\mathrm{disc}|$. The discriminatory part of the

rate results from interference effects, where process channels involving pseudovectors (magnetic transition dipole) interfere with process channels involving real vectors (electric transition dipole), such that their product changes its sign under spatial inversion. By using the free-space Green's tensor (A9) we find the following for the two rate contributions:

$$\Gamma_{\rm nd} = \frac{\rho}{36\pi\epsilon_0^2\hbar^2 r^6}\Bigg\{\left(\left|\boldsymbol{d}_{\rm e}^{\rm A}\right|^2\left|\boldsymbol{d}_{\rm e}^{\rm D}\right|^2 + \left|\boldsymbol{d}_{\rm m}^{\rm A}\right|^2\left|\boldsymbol{d}_{\rm m}^{\rm D}\right|^2\right) \times\left[3+\frac{\omega^2 r^2}{c^2}+\frac{\omega^4 r^4}{c^4}\right] + \left(\left|\boldsymbol{d}_{\rm e}^{\rm A}\right|^2\left|\boldsymbol{d}_{\rm m}^{\rm D}\right|^2 + \left|\boldsymbol{d}_{\rm m}^{\rm A}\right|^2\left|\boldsymbol{d}_{\rm e}^{\rm D}\right|^2\right) \times\left[\frac{\omega^2 r^2}{c^2}+\frac{\omega^4 r^4}{c^4}\right]\Bigg\}, \tag{37}$$

$$\Gamma_{\rm disc} = \rho\frac{R_{\rm D}R_{\rm A}}{18\pi c^2\epsilon_0^2\hbar^2 r^6}\left(3+2\frac{\omega^2 r^2}{c^2}+2\frac{\omega^4 r^4}{c^4}\right), \tag{38}$$

where $\omega = \omega_{\rm D}$ is the transition frequency. We define the degree of discrimination as

$$S = \frac{\Gamma_{\rm L}-\Gamma_{\rm R}}{\Gamma_{\rm L}+\Gamma_{\rm R}} = \frac{\Gamma_{\rm disc}}{\Gamma_{\rm nd}} \in [-1,1]. \tag{39}$$

Usually the magnetic dipole is much smaller than the electric one, i.e., $\boldsymbol{d}_{\rm m} \ll \boldsymbol{d}_{\rm e}$. With this approximation the degree of discrimination in free space is given by the simple expression

$$S \approx \frac{4R_{\rm D}R_{\rm A}}{c^2\left|\boldsymbol{d}_{\rm e}^{\rm A}\right|^2\left|\boldsymbol{d}_{\rm e}^{\rm D}\right|^2}\frac{3+2k_0^2r^2+2k_0^4r^4}{3+k_0^2r^2+k_0^4r^4}, \tag{40}$$

where $k_0 = \omega_{\rm D}/c$. It exhibits a lower bound $S_{r\to 0}$ in the nonretarded or near-zone limit of small separations and an upper bound $S_{r\to\infty}$ in the retarded or far-zone limit of large distances. These limits may be derived analytically, yielding

$$S_{r\to 0} \approx \frac{4R_{\rm D}R_{\rm A}}{c^2\left|\boldsymbol{d}_{\rm e}^{\rm A}\right|^2\left|\boldsymbol{d}_{\rm e}^{\rm D}\right|^2}, \tag{41}$$

$$S_{r\to\infty} \approx \frac{8R_{\rm D}R_{\rm A}}{c^2\left|\boldsymbol{d}_{\rm e}^{\rm A}\right|^2\left|\boldsymbol{d}_{\rm e}^{\rm D}\right|^2} = 2S_{r\to 0}. \tag{42}$$

Although the absolute rate rapidly decreases with increasing separation distance ($\sim r^{-6}$), the discrimination is stronger by a factor of approximately 2 in the far zone ($r\omega/c > 1$). This can be seen in Fig. 3, where the rate contributions and the degree of discrimination in free space as well as in a medium are plotted as a function of separation distance r between the donor and the acceptor for the example of 3MCP as the chiral donor and acceptor.

The transition frequency for 3MCP is given by $\omega = 6.44\times 10^{15}$ s^{-1} and as we can see in Fig. 3 the retarded limit is reached at separation distances of roughly $r = 2c/\omega \approx 100$ nm.

The chosen example of 3MCP features a transition with a very small electric transition dipole ($|\boldsymbol{d}_e| = 2.44\times 10^{-31}$ Cm) compared to its magnetic transition dipole ($|\boldsymbol{d}_m| = 3.31\times 10^{-32}$ Cm) [27,47–49]. This leads to a relatively large rotatory strength $R/c = \mathrm{Im}[\boldsymbol{d}_e\cdot\boldsymbol{d}_m]$. If we define an angle such that

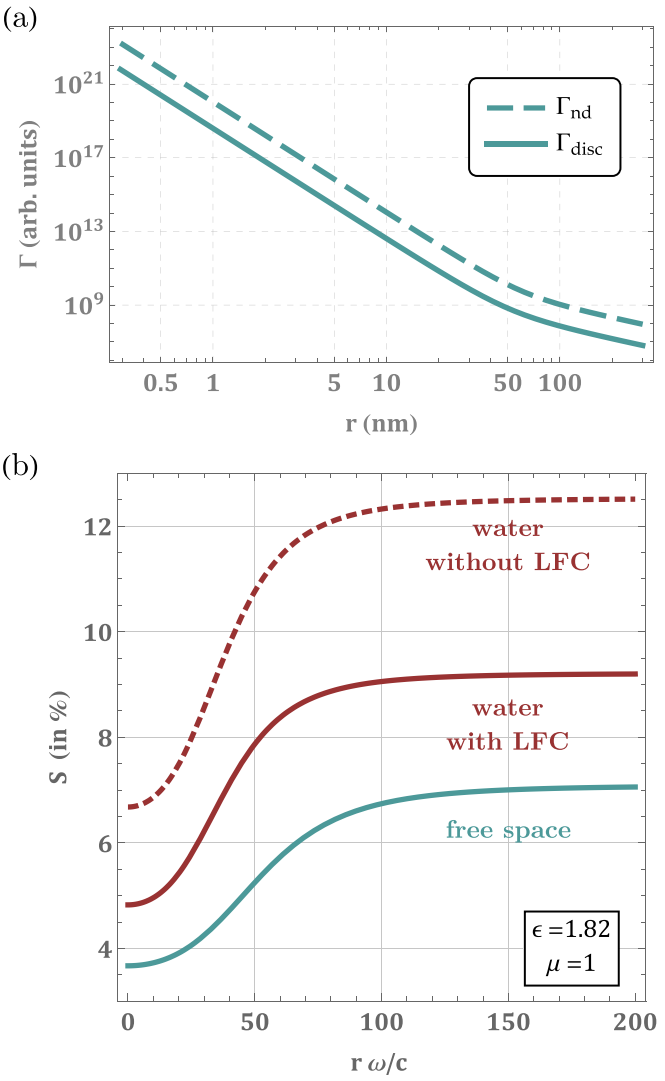

FIG. 3. (a) Discriminatory and nondiscriminatory rate contributions for RET in free space between chiral donor and acceptor as a function of their separation distance r on the example of 3MCP, as given by Eqs. (38) and (37). (b) Degree of discrimination $S = \Gamma_{\rm disc}/\Gamma_{\rm nd}$ for 3MCP as a function of separation distance r in free space, in water without the local field correction (LFC) (i.e., $c_{\rm e} = c_{\rm m} = 1$) and in water with local field correction [i.e., $c_{\rm e}$, $c_{\rm m}$ given by Eqs. (47)]. The rates $\Gamma_{\rm disc}$ and $\Gamma_{\rm nd}$ in media are given by Eqs. (48) and (49).

$R/c = |\boldsymbol{d}_e||\boldsymbol{d}_m|\cos\theta$, we find $\cos\theta = 0.98 \approx 1$ for 3MCP. Nonetheless, the maximum degree of discrimination in free space for 3MCP is only at $S = 7\%$. The chosen example is a chiral molecule whose properties are well known and which was used in a variety of similar studies with the aim of discrimination such as in Ref. [27]. This makes 3MCP an appropriate candidate system to demonstrate the discriminatory power of RET.

In Fig. 3 we also plot the enhanced degree of discrimination for 3MCP inside a medium with and without local field corrections. In the next section we derive the necessary formulas to consider such a surrounding medium and discuss the resulting effect on the discrimination.

IV. ENHANCED DISCRIMINATION IN MAGNETOELECTRIC MEDIUM

While in free space the degree of discrimination is completely determined by the molecules involved and their separation distance, we may modulate the effect by introducing a medium that surrounds the molecules. This can be either a liquid or a gas that is well described by its macroscopic properties. Let us consider a homogeneous magnetoelectric medium with relative permittivity and permeability $\varepsilon(\omega)$, $\mu(\omega) \neq 1$ that are in general complex-valued (see Fig. 1). We can easily include the impact of such a medium on the excitation propagation via the appropriate Green's tensor (A7) and the rate formula (27). The Green's tensor that fulfils the Helmholtz equation inside such a medium is given by

$$\mathbb{G}(\boldsymbol{r}_2, \boldsymbol{r}_1, \omega) = -\frac{\mu}{3k^2}\boldsymbol{\delta}(\boldsymbol{r}) - \frac{\mu e^{ikr}}{4\pi k^2 r^3}\{[1 - ikr - (kr)^2]\mathbb{I} - [3 - 3ikr - (kr)^2]\boldsymbol{e}_r \otimes \boldsymbol{e}_r\}, \tag{43}$$

with $\boldsymbol{r} = \boldsymbol{r}_2 - \boldsymbol{r}_1$, $k = \sqrt{\varepsilon\mu}\,\omega_{\mathrm{D}}/c$, and $\boldsymbol{e}_r = \boldsymbol{r}/r$. The applied formalism is suited to treat inhomogeneous media as well, where $\boldsymbol{\varepsilon}(\boldsymbol{r}, \omega)$ and $\boldsymbol{\mu}(\boldsymbol{r}, \omega)$ might be tensor-valued and position dependent. The Green's function that solves the respective Helmholtz equation might then not be known analytically but needs to be solved numerically. Using the definition of S (39), and evaluating the retarded and nonretarded limits, we find

$$S_{r\to 0} = \frac{4R_{\mathrm{D}}R_{\mathrm{A}}(\mathrm{Re}[n_r]^2 - \mathrm{Im}[n_r]^2)}{c^2\left(\left|\boldsymbol{d}_{\mathrm{e}}^{\mathrm{A}}\right|^2\left|\boldsymbol{d}_{\mathrm{e}}^{\mathrm{D}}\right|^2 + |n_r|^4\left|\boldsymbol{d}_{\mathrm{m}}^{\mathrm{A}}\right|^2\left|\boldsymbol{d}_{\mathrm{m}}^{\mathrm{D}}\right|^2\right)}, \tag{44}$$

$$S_{r\to\infty} = \frac{8R_{\mathrm{D}}R_{\mathrm{A}}\mathrm{Re}[n_r]^2}{c^2\left(\left|\boldsymbol{d}_{\mathrm{e}}^{\mathrm{A}}\right|^2 + |n_r|^2\left|\boldsymbol{d}_{\mathrm{m}}^{\mathrm{A}}\right|^2\right)\left(\left|\boldsymbol{d}_{\mathrm{e}}^{\mathrm{D}}\right|^2 + |n_r|^2\left|\boldsymbol{d}_{\mathrm{m}}^{\mathrm{D}}\right|^2\right)}, \tag{45}$$

where $n_r = \sqrt{\varepsilon\mu}$ is the medium's complex refractive index, and in contrast to the free-space case we did not neglect higher orders in $\boldsymbol{d}_{\mathrm{m}}$ to account for cases with $|n_r| \gg 1$. The free-space discrimination (40) can be recovered for $n_r = 1$.

However, it is known that this description is overly simplified. When embedding the microscopic system into the macroscopically described medium, local field effects around the donor and the acceptor as well as screening effects must be taken into account. Without these, the model would assume emission and absorption inside of the macroscopic medium, which is incorrect as the interactions with the field appear inside of the microscopically described molecules that are not permeated by a continuous medium. This so-called local field correction is, in fact, a necessity to correct the naive approach. There are a variety of different local field models [50,51]. The different models all take the local field effects into account by assuming the interacting atoms to be enclosed in a virtual or real spherical cavity surrounded by the medium, where the size of the introduced cavity is small compared to the relevant transition wavelength. In the virtual cavity model the introduced cavity is again filled microscopically by the atoms that form the medium. As a result, the macroscopic fields are not disturbed by the presence of the cavity. Here we employ the Onsager real cavity model [52], where infinitesimal empty regions around the emitting and absorbing atoms are assumed that influence the resulting macroscopic fields in contrast to the virtual cavity approach.

Which model is better suited depends on the setup at hand and is still under discussion. It is commonly presumed that a virtual cavity approach is rather suited for interstitial atoms, while a real cavity approach is often the right choice for substitutional atoms. In the case of a homogeneous magnetoelectric medium the correction via the Onsager real cavity model leads to additional factors to the dual Green's tensors. They differ depending on the nature of the interaction at each point (electric or magnetic) and are lowest-order transmission (Mie-)coefficients.

The local-field-corrected dual Green's tensor reads

$$\mathbb{G}^{\mathrm{lfc}}_{\lambda\lambda'} = c_\lambda \mathbb{G}_{\lambda\lambda'} c_{\lambda'}, \tag{46}$$

$$\text{with} \quad c_{\mathrm{e}} = \frac{3\varepsilon}{1+2\varepsilon} \quad \text{and} \quad c_{\mathrm{m}} = \frac{3}{1+2\mu}. \tag{47}$$

Using $\mathbb{G}^{\mathrm{lfc}}_{\lambda\lambda'}$ in the rate formula (27) we find the rate in such a medium including local field effects. The discriminatory and nondiscriminatory rate contributions are then given by

$$\Gamma_{\mathrm{disc}} = \frac{R_{\mathrm{A}}R_{\mathrm{D}}|\mu|^2 e^{-2\mathrm{Im}n_r\, k_0 r}}{18\pi c^2 r^6 \varepsilon_0^2 \hbar^2 |n_r|^4}\{k_0^2 r^2 |c_{\mathrm{e}}|^2 |c_{\mathrm{m}}|^2 |n_r|^4 \left(k_0^2 r^2 |n_r|^2 + 2k_0 r \mathrm{Im}n_r + 1\right) + \mathrm{Re}\left[c_{\mathrm{e}}^{*2} c_{\mathrm{m}}^2 n_r^2\right]\left(k_0^2 r^2 |n_r|^2 (2k_0 r \mathrm{Im}n_r + 1) + k_0^4 r^4 |n_r|^4 + k_0^2 r^2 \mathrm{Im}n_r^2 + 6k_0 r \mathrm{Im}n_r + 3\right)\}, \tag{48}$$

$$\Gamma_{\mathrm{nd}} = \frac{|\mu|^2 \left|\boldsymbol{d}_{\mathrm{e}}^{\mathrm{A}}\right|^2 \left|\boldsymbol{d}_{\mathrm{e}}^{\mathrm{D}}\right|^2 e^{-2\mathrm{Im}n_r\, k_0 r}}{36\pi r^6 \varepsilon_0^2 \hbar^2 |n_r|^4}\Bigg\{|c_{\mathrm{e}}|^4\left(|n_r|^4 k_0^4 r^4 + |n_r|^2 k_0^2 r^2 (2\mathrm{Im}n_r k_0 r + 1) + 4\mathrm{Im}n_r^2 k_0^2 r^2 + 6\mathrm{Im}n_r k_0 r + 3\right) + |c_{\mathrm{e}}|^2 |n_r c_{\mathrm{m}}|^2 \left(\frac{\left|\boldsymbol{d}_{\mathrm{m}}^{\mathrm{D}}\right|^2}{\left|\boldsymbol{d}_{\mathrm{e}}^{\mathrm{D}}\right|^2} + \frac{\left|\boldsymbol{d}_{\mathrm{m}}^{\mathrm{A}}\right|^2}{\left|\boldsymbol{d}_{\mathrm{e}}^{\mathrm{A}}\right|^2}\right)\left(2|n_r|^4 k_0^4 r^4 + |n_r|^2 k_0^2 r^2 (2\mathrm{Im}n_r k_0 r + 1)\right) + \left|n_r c_{\mathrm{m}}\right|^4 \frac{\left|\boldsymbol{d}_{\mathrm{m}}^{\mathrm{D}}\right|^2 \left|\boldsymbol{d}_{\mathrm{m}}^{\mathrm{A}}\right|^2}{\left|\boldsymbol{d}_{\mathrm{e}}^{\mathrm{D}}\right|^2 \left|\boldsymbol{d}_{\mathrm{e}}^{\mathrm{A}}\right|^2}\left(|n_r|^2 k_0^2 r^2 (2\mathrm{Im}n_r k_0 r + 1) + |n_r|^4 k_0^4 r^4 + 4\mathrm{Im}n_r^2 k_0^2 r^2 + 6\mathrm{Im}n_r k_0 r + 3\right)\Bigg\}, \tag{49}$$

where $k_0 = \omega_{\mathrm{D}}/c$ and Γ_{nd} reduces to the known electric dipole-dipole RET rate for $|\boldsymbol{d}_m| = 0$ [32,42].

By dividing Eq. (48) by Eq. (49) and performing the limit of small and large distances, respectively, we obtain the degree of discrimination in its retarded and nonretarded limits. For general magnetoelectric media including local field effects, they are given by

$$S^{\mathrm{lfc}}_{r\to 0} = \frac{4R_{\mathrm{D}}R_{\mathrm{A}}}{D^{\mathrm{lfc}}_{0}}\mathrm{Re}[(c_{\mathrm{e}}^{*}c_{\mathrm{m}}n_r)^2], \tag{50}$$

$$D^{\mathrm{lfc}}_{0} = c^2\big(|c_{\mathrm{e}}|^2\big|\boldsymbol{d}^{\mathrm{A}}_{\mathrm{e}}\big|^2\big|\boldsymbol{d}^{\mathrm{D}}_{\mathrm{e}}\big|^2 + |c_{\mathrm{m}}|^2|n_r|^4\big|\boldsymbol{d}^{\mathrm{A}}_{\mathrm{m}}\big|^2\big|\boldsymbol{d}^{\mathrm{D}}_{\mathrm{m}}\big|^2\big), \tag{51}$$

$$S^{\mathrm{lfc}}_{r\to \infty} = \frac{8R_{\mathrm{D}}R_{\mathrm{A}}}{D^{\mathrm{lfc}}_{\infty}}\mathrm{Re}[c_{\mathrm{e}}^{*}c_{\mathrm{m}}n_r]^2, \tag{52}$$

$$D^{\mathrm{lfc}}_{\infty} = c^2\big(|c_{\mathrm{e}}|^2\big|\boldsymbol{d}^{\mathrm{A}}_{\mathrm{e}}\big|^2 + |c_{\mathrm{m}}|^2|n_r|^2\big|\boldsymbol{d}^{\mathrm{A}}_{\mathrm{m}}\big|^2\big)\big(|c_{\mathrm{e}}|^2\big|\boldsymbol{d}^{\mathrm{D}}_{\mathrm{e}}\big|^2 + |c_{\mathrm{m}}|^2|n_r|^2\big|\boldsymbol{d}^{\mathrm{D}}_{\mathrm{m}}\big|^2\big), \tag{53}$$

where for each electric and magnetic transition dipole moment there appears an electric correction factor c_{e} and a magnetic correction c_{m}, respectively. The uncorrected case can be recovered for $c_{\mathrm{e}} = c_{\mathrm{m}} = 1$ and the free-space case for $\varepsilon = \mu = n_r = 1$. In Fig. 3 the degree of discrimination is shown with and without correction for water with real permittivity $\varepsilon(\omega) \approx 1.82$ and trivial permeability $\mu(\omega) = 1$ (i.e., $n_r \approx 1.35$). As demonstrated in Fig. 3, for our example, the impact of the local field correction is of similar magnitude as the impact of the medium itself compared to the free-space case. Without corrections, the medium's impact on the degree of discrimination would be overestimated here. However, even in water the degree of discrimination is enhanced by roughly 30%. An appropriate medium may enhance the degree of discrimination, in general, up to $S = \prod_{\mathrm{X}} \mathrm{Im}[\boldsymbol{d}^{\mathrm{X}}_{\mathrm{m}} \cdot \boldsymbol{d}^{\mathrm{X}}_{\mathrm{e}}]/|\boldsymbol{d}^{\mathrm{X}}_{\mathrm{m}}||\boldsymbol{d}^{\mathrm{X}}_{\mathrm{e}}| = \prod_{\mathrm{X}} \cos\theta_{\mathrm{X}} \leqslant 100\%$, where $\mathrm{X} \in \{\mathrm{A}, \mathrm{D}\}$. A degree of discrimination of 100% corresponds then to vanishing excitation transfer to the opposite-handed acceptor ($\Gamma_{\mathrm{R}} = 0$ for a left-handed donor) independent of the separation distance. It can only be achieved for $\theta = 0$. This is approximately the case in the chosen example of 3MCP. If we limit ourselves to positive real refractive indices $n_r > 0$ with trivial permeabilities $\mu \approx 1$, the maximum enhancement can be achieved for 3MCP at $n_{r,\max} \approx 11$ and, alternatively but less relevant, at $n_{r,\max} \approx 0.045$ (see Fig. 4). It is interesting to note that the discrimination vanishes in the limit $n_r \to \infty$. We can predict the maximum real refractive indices at which $S = \cos^2\theta$ for any two chiral molecules of the same kind as a function of the ratio $|\boldsymbol{d}_{\mathrm{e}}|/|\boldsymbol{d}_{\mathrm{m}}|$, as shown in Fig. 4. They are given by

$$n_{r,\max} = \frac{3}{4}\frac{|\boldsymbol{d}_{\mathrm{e}}|}{|\boldsymbol{d}_{\mathrm{m}}|}\left(1 \pm \frac{\sqrt{9 - 8\frac{|\boldsymbol{d}_{\mathrm{m}}|}{|\boldsymbol{d}_{\mathrm{e}}|}}}{4}\right). \tag{54}$$

The smaller the ratio the closer both optimum refractive indices are to unity. In Fig. 5 we present the nonretarded and retarded degrees of discrimination $S_{r\to 0/\infty}$ as functions of a complex refractive index. In theory, one may achieve a complete inversion of the discriminatory effect in the nonretarded limit for $\mathrm{Im}n_r \gg \mathrm{Re}n_r$. In the chosen example of 3MCP, the same-handed rate vanishes, $\Gamma_{\mathrm{L}} = 0 \Leftrightarrow S_{r\to 0} = -100\%$, for $\mathrm{Im}n_r = 11$ and $\mathrm{Im}n_r = 0.045$. However, the retarded limit does not experience such an inversion of the effect. Here the discrimination simply vanishes with larger $\mathrm{Im}n_r$. Most conventional media may be found around $1 < \mathrm{Re}n_r < 2$ and $0 < \mathrm{Im}n_r \ll 1$. At the transition frequency of 3MCP ($\omega_{\mathrm{D}} = 6.44 \times 10^{15}\ \mathrm{s}^{-1} = 4.3\,\mathrm{eV}$), some example media are given in Table I [53]. If possible, their refractive indices were marked in Fig. 5. An interesting simple medium example is mercury where the discrimination is inverted in the nonretarded limit compared to the free-space case. Solutions with resonances at the desired frequency as well as fluids based on metamaterials may be engineered to cover a larger range of the presented parameter space [54]. The choice of an appropriate medium then depends highly on the transition frequency.

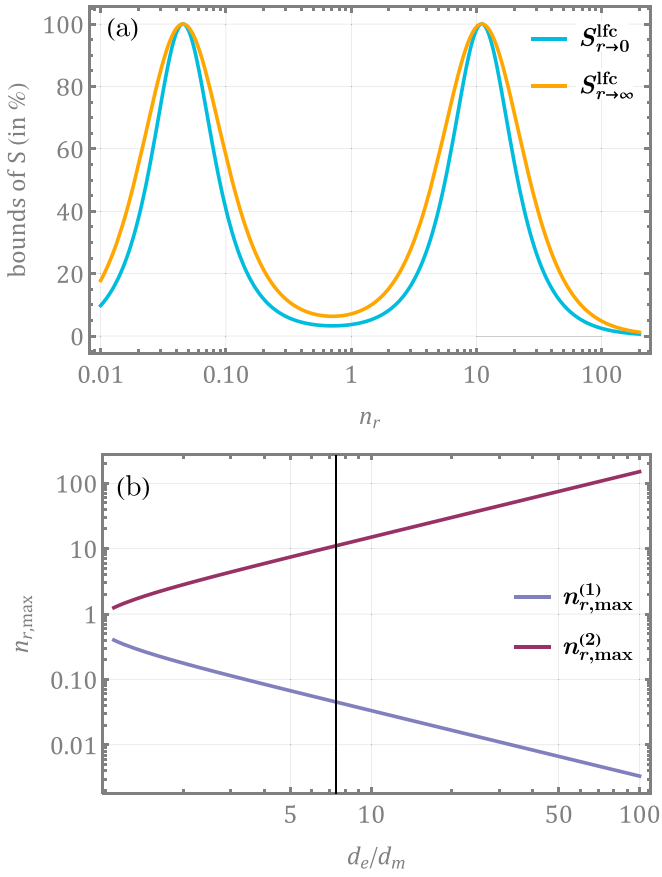

FIG. 4. (a) Upper and lower bound of S for 3MCP in a dielectric medium given by Eqs. (50) and (52). (b) Real refractive index of a dielectric medium for maximum discrimination as a function of the molecule's transition dipole ratio. The solid line marks the ratio for 3MCP.

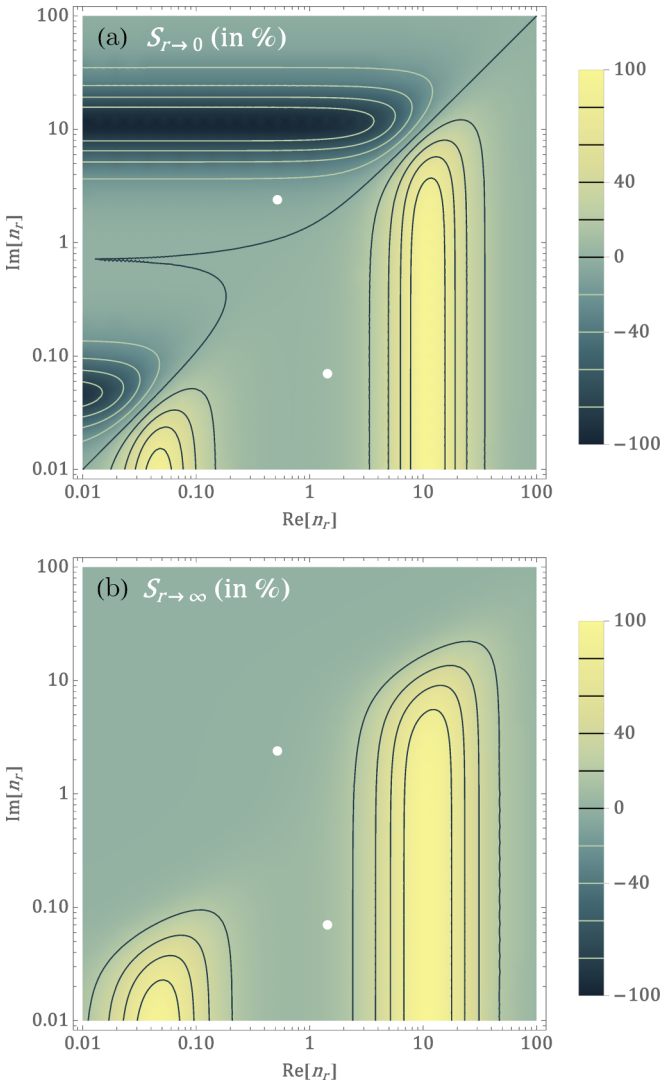

FIG. 5. Nonretarded (a) and retarded (b) degrees of discrimination as a function of real and imaginary parts of the refractive index (with $\mu = 1$) for the example of 3MCP. We marked simple media with complex n_r: methane at $n_r = 1.44 + 0.04i$ and mercury at $n_r = 0.52 + 2.39i$.

V. CONCLUSION

We derived the RET rate between chiral molecules in the framework of macroscopic QED, which includes retardation effects and is able to take the impact of different environments into account. Although the considered system consists of one donor and one acceptor molecule, the extension to N molecules is straightforward. The rate differs between same- and opposite-handed enantiomers, making the rate discriminatory. The degree of discrimination is usually larger in the far zone, also known as the retarded limit of large intermolecular separation distances. However, this constitutes a trade-off between the degree of discrimination and the overall energy transfer rate, which decreases rapidly with increasing separation distance. We showed that putting the system inside a magnetoelectric medium can have significant effects on the discrimination. In one example we demonstrated the significant impact of local field and screening effects on the prediction of the degree of discrimination. Here, we chose the Onsager real cavity model to account for these effects. We offered analytical expressions for the rate involving chiral molecules in a magnetoelectric medium including local field effects. We applied our theory to the example of 3-methylcyclopentanone (3MCP). By putting the system inside water the degree of discrimination between two chiral 3MCP molecules is already enhanced by roughly 30%.

We studied a large complex parameter space for dielectric media and showed that appropriate media may even lead to perfect discrimination; i.e., the energy transfer to the opposite-handed enantiomer is completely suppressed. The degree of discrimination shows, in general, two such maxima for real refractive indices. One of these optimal refractive indices is much larger than unity, and the other is much smaller, depending on the transition dipoles involved in the process. The smaller the ratio between electric and magnetic transition dipole moments the closer the optimal refractive indices are to unity. Media with a large imaginary refractive index can even invert the effect in the near-zone or nonretarded limit of small separation distances, such that the opposite-handed enantiomer instead of the same-handed one is preferred by the process. The medium imprints a complex phase onto the propagated field excitation; this phase change might differ for the magnetic and electric components and hence also invert the sign of the interference terms between the two, which build up the discriminatory contribution of the rate. In general, an imaginary refractive index corresponds to strong absorption in the medium. The medium's macroscopic properties are evaluated at the molecule's transition frequency. Hence, the best choice for a medium depends on the molecules of interest. We offered some simple example media at the transition frequency of 3MCP. The transition frequency of the chosen example molecule is quite large and simple liquids show little optical response. However, for vibrational transitions involving wavelengths in the IR regime, recent advancements in the field of metamaterials could soon offer media that will explore a larger area of the presented parameter space.

In this work we chose chiral molecules and an achiral environment. However, even macroscopic media can have chiral features. Although the environment only passively takes part in the energy transfer process, its chiral property might be able to actively discriminate enantiomers. Here, we employed the Onsager real cavity model to account for local field and screening effects. For some systems alternative local field models are more suited. Their influence on the discrimination will be studied in future work.

TABLE I. Table of different simple media, their respective refractive index, and their degree of discrimination in the nonretarded and retarded limits [53].

Medium	Refractive index	$S_{r\to 0}$	$S_{r\to\infty}$
Water	$1.4 + 10^{-8}i$	5.04%	9.60%
Biodiesel	$1.56 + 8 \times 10^{-6}i$	5.85%	11.06%
Ethanol	$1.39 + 3 \times 10^{-6}i$	5.01%	9.55%
Methane	$1.44 + 0.07i$	5.19%	9.87%
Mercury	$0.52 + 2.39i$	−7.30%	0.96%

ACKNOWLEDGMENTS

The authors thank R. Bennett for discussions. This work was supported by the German Research Foundation (DFG, Grants No. BU 1803/3-1 and No. GRK 2079/1 and DFG, Project No. 328961117-SFB 1319 ELCH).

APPENDIX A: GREEN'S TENSOR

The Fourier components of the electric field are given by Eq. (10) with the shorthand notation

$$\mathbb{G}_{\mathrm{e}}(\boldsymbol{r},\boldsymbol{r}',\omega)=i\frac{\omega^2}{c^2}\sqrt{\frac{\hbar}{\pi\varepsilon_0}\mathrm{Im}\varepsilon(\boldsymbol{r}',\omega)}\mathbb{G}(\boldsymbol{r},\boldsymbol{r}',\omega), \tag{A1}$$

$$\mathbb{G}_{\mathrm{m}}(\boldsymbol{r},\boldsymbol{r}',\omega)=-i\frac{\omega}{c}\sqrt{\frac{\hbar}{\pi\varepsilon_0}\frac{\mathrm{Im}\mu(\boldsymbol{r}',\omega)}{|\mu(\boldsymbol{r}',\omega)|^2}}\mathbb{G}(\boldsymbol{r},\boldsymbol{r}',\omega)\times\overleftarrow{\nabla}'. \tag{A2}$$

Note that they are not related to the dual definition $\mathbb{G}_{\lambda\lambda'}$ for the Green's tensor but are shorthand notations that are often used in the field of macroscopic QED. From Eq. (10) it follows that the Green's tensor $\mathbb{G}$ must fulfil the Helmholtz equation

$$\left[\overrightarrow{\nabla}_a\times\frac{1}{\mu(\boldsymbol{r}_a,\omega)}\overrightarrow{\nabla}_a\times-\frac{\omega^2}{c^2}\varepsilon(\boldsymbol{r}_a,\omega)\right]\mathbb{G}(\boldsymbol{r}_a,\boldsymbol{r}_b,\omega)=\boldsymbol{\delta}(\boldsymbol{r}_a-\boldsymbol{r}_b). \tag{A3}$$

When considering homogeneous media it is sufficient to solve the scalar Helmholtz equation

$$-[\Delta_a+k^2]g(\boldsymbol{r}_a,\boldsymbol{r}_b,\omega)=\delta(\boldsymbol{r}_a-\boldsymbol{r}_b), \tag{A4}$$

with $k^2=\epsilon\mu\omega/c$. It is solved by the scalar Green's function

$$g(\boldsymbol{r}_a,\boldsymbol{r}_b,\omega)=\frac{e^{ik|\boldsymbol{r}_a-\boldsymbol{r}_b|}}{4\pi|\boldsymbol{r}_a-\boldsymbol{r}_b|}. \tag{A5}$$

The Green's tensor is then given by the Green's function g via

$$\mathbb{G}(\boldsymbol{r}_a,\boldsymbol{r}_b,\omega)=\mu\left[\mathbb{I}+\frac{1}{k^2}\overrightarrow{\nabla}_a\otimes\overrightarrow{\nabla}_a\right]g(\boldsymbol{r}_a,\boldsymbol{r}_b,\omega), \tag{A6}$$

and yields with g given by Eq. (A5)

$$\mathbb{G}(\boldsymbol{r}_a,\boldsymbol{r}_b,\omega)=-\frac{\mu}{3k^2}\boldsymbol{\delta}(\boldsymbol{r})-\frac{\mu e^{ikr}}{4\pi k^2r^3}\{[1-ikr-k^2r^2]\mathbb{I}-[3-3ikr-k^2r^2]\boldsymbol{e}_r\otimes\boldsymbol{e}_r\}, \tag{A7}$$

with $\boldsymbol{r}=\boldsymbol{r}_a-\boldsymbol{r}_b$ and $\boldsymbol{e}_r=\boldsymbol{r}/r$. In free space ($\epsilon=\mu=1$), we hence find

$$\mathbb{G}^{(0)}(\boldsymbol{r}_a,\boldsymbol{r}_b,\omega)=\left[\mathbb{I}+\frac{c^2}{\omega^2}\overrightarrow{\nabla}_a\otimes\overrightarrow{\nabla}_a\right]\frac{e^{i\omega|\boldsymbol{r}_a-\boldsymbol{r}_b|/c}}{4\pi|\boldsymbol{r}_a-\boldsymbol{r}_b|} \tag{A8}$$

$$=-\frac{1}{3k_0^2}\boldsymbol{\delta}(\boldsymbol{r})-\frac{e^{ik_0r}}{4\pi k_0^2r^3}\left\{\left[1-\mathrm{i}k_0r-k_0^2r^2\right]\mathbb{I}-\left[3-3ik_0r-k_0^2r^2\right]\boldsymbol{e}_r\otimes\boldsymbol{e}_r\right\}. \tag{A9}$$

APPENDIX B: DERIVATION OF TRANSITION MATRIX ELEMENTS

Using the formula for the transition matrix element (4) with the interaction Hamiltonian (2), the initial and final states given by $|i\rangle=|1\rangle_{\mathrm{D}}|0\rangle_{\mathrm{A}}|\{0\}\rangle_F$ and $|f\rangle=|0\rangle_{\mathrm{D}}|1\rangle_{\mathrm{A}}|\{0\}\rangle_F$, and the introduced dual notation [see Eq. (28a)] leads to the following expression:

$$M=-\int d\omega'\int d^3r'\sum_{\{\lambda\}}\left[\langle g|\hat{\boldsymbol{d}}^{\mathrm{D}}_{\lambda_1}|e\rangle_{\mathrm{D}}\cdot\frac{\langle\{0\}|\hat{\boldsymbol{E}}_{\lambda_1}(\boldsymbol{r}_{\mathrm{D}})|\mathbf{1}'\rangle_{\mathrm{F}}\langle\mathbf{1}'|\hat{\boldsymbol{E}}_{\lambda_2}(\boldsymbol{r}_{\mathrm{A}})|\{0\}\rangle_{\mathrm{F}}}{\hbar\omega'+\hbar\omega_{\mathrm{A}}}\cdot\langle 1|\hat{\boldsymbol{d}}^{\mathrm{A}}_{\lambda_2}|0\rangle_{\mathrm{A}}\right.$$
$$\left.+\langle 1|\hat{\boldsymbol{d}}^{\mathrm{A}}_{\lambda_1}|0\rangle_{\mathrm{A}}\cdot\frac{\langle\{0\}|\hat{\boldsymbol{E}}_{\lambda_1}(\boldsymbol{r}_{\mathrm{A}})|\mathbf{1}'\rangle_{\mathrm{F}}\langle\mathbf{1}'|\hat{\boldsymbol{E}}_{\lambda_2}(\boldsymbol{r}_{\mathrm{D}})|\{0\}\rangle_{\mathrm{F}}}{\hbar\omega'-\hbar\omega_{\mathrm{D}}}\cdot\langle g|\hat{\boldsymbol{d}}^{\mathrm{D}}_{\lambda_2}|e\rangle_{\mathrm{D}}\right], \tag{B1}$$

where $\hat{\boldsymbol{E}}_{\mathrm{e}}=\hat{\boldsymbol{E}}$ and $\hat{\boldsymbol{E}}_{\mathrm{m}}=c\hat{\boldsymbol{B}}$. It is trivial to write the matrix element in a nondual formulation. However, the dual definitions offer a simplified notation. By introducing the projection onto the frequency subspace,

$$\hat{P}(\omega)=\sum_{n,\lambda}\int d^3r\,|\boldsymbol{n}_\lambda(\boldsymbol{r},\omega)\rangle\langle\boldsymbol{n}_\lambda(\boldsymbol{r},\omega)|, \tag{B2}$$

each term in Eq. (B1) can be written as

$$\int d\omega'\int d^3r'\sum_{\lambda'}\frac{\langle\{0\}|\hat{\boldsymbol{E}}_{\lambda_1}(\boldsymbol{r}_\alpha)|\mathbf{1}'\rangle\langle\mathbf{1}'|\hat{\boldsymbol{E}}_{\lambda_2}(\boldsymbol{r}_\beta)|\{0\}\rangle}{\hbar\omega'+\hbar\omega}$$
$$=\int d\omega'\int d^3r'\sum_{\lambda',n}\frac{\langle\{0\}|\hat{\boldsymbol{E}}_{\lambda_1}(\boldsymbol{r}_\alpha)|\boldsymbol{n}'\rangle\langle\boldsymbol{n}'|\hat{\boldsymbol{E}}_{\lambda_2}(\boldsymbol{r}_\beta)|\{0\}\rangle}{\hbar\omega'+\hbar\omega}$$
$$=\int d\omega'\frac{\langle\{0\}|\hat{\boldsymbol{E}}_{\lambda_1}(\boldsymbol{r}_\alpha)\hat{P}(\omega')\hat{\boldsymbol{E}}_{\lambda_2}(\boldsymbol{r}_\beta)|\{0\}\rangle}{\hbar\omega'+\hbar\omega}$$
$$=\int d\omega_1\int d\omega_2\frac{\left\langle\hat{\boldsymbol{E}}_{\lambda_1}(\boldsymbol{r}_\alpha,\omega_1)\hat{\boldsymbol{E}}^{\dagger}_{\lambda_2}(\boldsymbol{r}_\beta,\omega_2)\right\rangle}{\hbar\omega_2+\hbar\omega}, \tag{B3}$$

where $\langle\cdot\rangle$ is the field vacuum's expectation value. The correlation functions $\langle\hat{\boldsymbol{E}}_{\lambda_1}(\boldsymbol{r}_\alpha,\omega_1)\hat{\boldsymbol{E}}^\dagger_{\lambda_2}(\boldsymbol{r}_\beta,\omega_2)\rangle$ can be evaluated by considering the field's expansion in terms of the Green's tensor (9)–(12). For the magnetic-electric correlation function (16), we find

$$\begin{aligned}
&\langle\hat{\boldsymbol{E}}_m(\boldsymbol{r}_a,\omega)\otimes\hat{\boldsymbol{E}}^\dagger_e(\boldsymbol{r}_b,\omega')\rangle\\
&\quad= c\,\langle\hat{\boldsymbol{B}}(\boldsymbol{r}_a,\omega)\otimes\hat{\boldsymbol{E}}^\dagger(\boldsymbol{r}_b,\omega')\rangle\\
&\quad= \sum_{\lambda,\lambda'}\iint d^3r'd^3r\frac{c}{i\omega}\Big\langle\overrightarrow{\nabla}_a\times\mathbb{G}_\lambda(\boldsymbol{r}_a,\boldsymbol{r},\omega)\cdot\hat{\boldsymbol{f}}_\lambda(\boldsymbol{r},\omega)\\
&\qquad\otimes\hat{\boldsymbol{f}}^\dagger_{\lambda'}(\boldsymbol{r}',\omega')\cdot\mathbb{G}^*_{\lambda'}(\boldsymbol{r}',\boldsymbol{r}_b,\omega')\Big\rangle\\
&\quad= \frac{\omega c}{i}\frac{\hbar\mu_0}{\pi}\delta(\omega-\omega')\overrightarrow{\nabla}_a\times\mathrm{Im}\mathbb{G}(\boldsymbol{r}_a,\boldsymbol{r}_b,\omega).
\end{aligned}\tag{B4}$$

The remaining correlation functions of Eqs. (14)–(17) follow analogously.

APPENDIX C: POLE INTEGRATION

Here we show how the relation Eq. (19) is obtained. In the derivation of all matrix elements of interest we encounter integrals in the frequency domain in the form of

$$\lim_{\epsilon\to0^+}\int d\omega\left\{\frac{f(\omega)}{\omega-(\omega_\mathrm{D}+i\epsilon)}+\frac{f(-\omega)}{\omega+\omega_\mathrm{A}}\right\}\mathrm{Im}\mathbb{G}(\omega),\tag{C1}$$

with $f(\omega)=\omega^n$, $n\in\{0,1,2\}$. Let us transform the first term in Eq. (C1). With the Schwarz-reflection principle $\mathbb{G}^*(\omega)=\mathbb{G}(-\omega^*)$, we find

$$\begin{aligned}
\int_0^\infty d\omega\frac{f(\omega)\mathrm{Im}\mathbb{G}(\omega)}{\omega-(\omega_\mathrm{D}+i\epsilon)}&=\frac{1}{2i}\int_0^\infty d\omega f(\omega)\frac{\mathbb{G}(\omega)}{\omega-(\omega_\mathrm{D}+i\epsilon)}\\
&\quad-\frac{1}{2i}\int_0^\infty d\omega f(\omega)\frac{\mathbb{G}(-\omega)}{\omega-(\omega_\mathrm{D}+i\epsilon)}\\
&=\frac{1}{2i}\left[\oint d\omega-\int_\Omega d\omega-\int_{-\infty}^0 d\omega\right]f(\omega)\frac{\mathbb{G}(\omega)}{\omega-(\omega_\mathrm{D}+i\epsilon)}\\
&\quad+\frac{1}{2i}\int_{-\infty}^0 d\omega f(-\omega)\frac{\mathbb{G}(\omega)}{\omega+(\omega_\mathrm{D}+i\epsilon)},
\end{aligned}\tag{C2}$$

where we express the integration as the sum over different integration paths in the complex plane (see Fig. 6). The closed path can be evaluated via the residuum theorem and the integration over path Ω vanishes since the Green's tensor is analytic in the upper half of the complex plane and vanishes

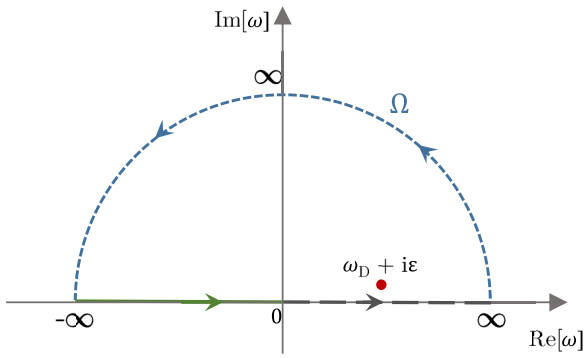

FIG. 6. Complex contour for the pole integration. The closed contour consists of the sum of the green contour (from $-\infty$ to 0), the gray contour (from 0 to ∞), and the blue dashed contour (Ω). It encloses a pole at $\omega=\omega_\mathrm{D}+i\epsilon$.

sufficiently fast for $\omega\to i\infty$, such that

$$\begin{aligned}
&\int_0^\infty d\omega\frac{f(\omega)\mathrm{Im}\mathbb{G}(\omega)}{\omega-(\omega_\mathrm{D}+i\epsilon)}\\
&\quad=\pi f(\omega_\mathrm{D}+i\epsilon)\mathbb{G}(\omega_\mathrm{D}+i\epsilon)\\
&\qquad-\frac{1}{2i}\int_{-\infty}^0 d\omega f(\omega)\frac{\mathbb{G}(\omega)}{\omega-(\omega_\mathrm{D}+i\epsilon)}\\
&\qquad+\frac{1}{2i}\int_{-\infty}^0 d\omega f(-\omega)\frac{\mathbb{G}(\omega)}{\omega+(\omega_\mathrm{D}+i\epsilon)}.
\end{aligned}\tag{C3}$$

The last integral in Eq. (C3) has no pole in the upper half of the complex plane. Substituting here the integration path similarly according to Fig. 6, i.e., $\int_{-\infty}^0\to\oint-\int_\Omega-\int_0^\infty$, leads to a single nonvanishing contribution: the closed contour vanishes due to a lack of enclosed poles and the integration over path Ω vanishes due to the properties of $\mathbb{G}$ on the upper half of the complex plane, and we are left with

$$\begin{aligned}
&\int_0^\infty d\omega\frac{f(\omega)\mathrm{Im}\mathbb{G}(\omega)}{\omega-(\omega_\mathrm{D}+i\epsilon)}\\
&\quad=\pi f(\omega_\mathrm{D}+i\epsilon)\mathbb{G}(\omega_\mathrm{D}+i\epsilon)\\
&\qquad-\frac{1}{2i}\int_{-\infty}^0 d\omega f(\omega)\frac{\mathbb{G}(\omega)}{\omega-(\omega_\mathrm{D}+i\epsilon)}\\
&\qquad-\frac{1}{2i}\int_0^\infty d\omega f(-\omega)\frac{\mathbb{G}(\omega)}{\omega+(\omega_\mathrm{D}+i\epsilon)}\\
&\quad=\pi f(\omega_\mathrm{D}+i\epsilon)\mathbb{G}(\omega_\mathrm{D}+i\epsilon)\\
&\qquad-\int_0^\infty d\omega f(-\omega)\frac{\mathrm{Im}\mathbb{G}(\omega)}{\omega+(\omega_\mathrm{D}+i\epsilon)},
\end{aligned}\tag{C4}$$

where we have used the Schwarz-reflection principle $\mathbb{G}(-\omega^*)=\mathbb{G}^*(\omega)$ again in the last step. This result is finite for $\epsilon\to0$, we may hence form the limit. Substituting this result back into our original expression (C1) reveals

$$\int_0^\infty d\omega\left(\frac{f(\omega)}{\omega-\omega_\mathrm{D}}+\frac{f(-\omega)}{\omega+\omega_\mathrm{A}}\right)\mathrm{Im}\mathbb{G}(\omega)=\pi f(\omega_\mathrm{D})\mathbb{G}(\omega_\mathrm{D}),\tag{C5}$$

for $\omega_\mathrm{A}=\omega_\mathrm{D}$.

[1] S. Y. Buhmann and D.-G. Welsch, Prog. Quantum Electron. **31**, 51 (2007).

[2] S. Scheel and S. Y. Buhmann, Acta Phys. Slovaca **58**, 675 (2008).

[3] S. Y. Buhmann, *Dispersion Forces I: Macroscopic Quantum Electrodynamics and Ground-State Casimir, Casimir–Polder and van der Waals Forces*, Springer Tracts in Modern Physics, Vol. 247 (Springer, Berlin, 2012).

[4] S. Y. Buhmann, *Dispersion Forces II: Many-Body Effects, Excited Atoms, Finite Temperature and Quantum Friction*, Springer Tracts in Modern Physics, Vol. 248 (Springer, Berlin, 2012).

[5] H. Safari, P. Barcellona, S. Y. Buhmann, and A. Salam, New J. Phys. **22**, 053049 (2020).

[6] M. Du, L. A. Martínez-Martínez, R. F. Ribeiro, Z. Hu, V. M. Menon, and J. Yuen-Zhou, Chem. Sci. **9**, 6659 (2018).

[7] A. Mandal and P. Huo, J. Phys. Chem. Lett. **10**, 5519 (2019).

[8] F. Herrera and J. Owrutsky, J. Chem. Phys. **152**, 100902 (2020).

[9] D. N. Basov, A. Asenjo-Garcia, P. J. Schuck, X. Zhu, and A. Rubio, Nanophotonics **10**, 549 (2021).

[10] T. E. Li, B. Cui, J. E. Subotnik, and A. Nitzan, Annu. Rev. Phys. Chem. **73**, 43 (2022).

[11] J. Fregoni, F. J. Garcia-Vidal, and J. Feist, ACS Photonics **9**, 1096 (2022).

[12] J. Yuen-Zhou, W. Xiong, and T. Shegai, J. Chem. Phys. **156**, 030401 (2022).

[13] S. Wang, G. D. Scholes, and L.-Y. Hsu, J. Chem. Phys. **151**, 014105 (2019).

[14] S. Wang, M.-W. Lee, Y.-T. Chuang, G. D. Scholes, and L.-Y. Hsu, J. Chem. Phys. **153**, 184102 (2020).

[15] J. Feist, A. I. Fernández-Domínguez, and F. J. García-Vidal, Nanophotonics **10**, 477 (2021).

[16] J. L. Hemmerich, R. Bennett, and S. Y. Buhmann, Nat. Commun. **9**, 2934 (2018).

[17] R. Bennett, P. Votavová, P. c. v. Kolorenč, T. Miteva, N. Sisourat, and S. Y. Buhmann, Phys. Rev. Lett. **122**, 153401 (2019).

[18] T. Jahnke, U. Hergenhahn, B. Winter, R. Dörner, U. Frühling, P. V. Demekhin, K. Gokhberg, L. S. Cederbaum, A. Ehresmann, A. Knie, and A. Dreuw, Chem. Rev. **120**, 11295 (2020).

[19] L. S. Cederbaum and A. I. Kuleff, Nat. Commun. **12**, 4083 (2021).

[20] J. Franz, R. Bennett, and S. Y. Buhmann, Phys. Rev. A **104**, 013103 (2021).

[21] J. Franz and S. Y. Buhmann, New J. Phys. **24**, 043002 (2022).

[22] A. Salam, J. Chem. Phys. **124**, 014302 (2006).

[23] D. S. Bradshaw and D. L. Andrews, New J. Phys. **16**, 103021 (2014).

[24] R. P. Cameron, S. M. Barnett, and A. M. Yao, New J. Phys. **16**, 013020 (2014).

[25] K. A. Forbes and D. L. Andrews, Phys. Rev. A **91**, 053824 (2015).

[26] P. Barcellona, H. Safari, A. Salam, and S. Y. Buhmann, Phys. Rev. Lett. **118**, 193401 (2017).

[27] F. Suzuki, T. Momose, and S. Y. Buhmann, Phys. Rev. A **99**, 012513 (2019).

[28] C. Genet, ACS Photonics **9**, 319 (2022).

[29] K. Nasiri Avanaki, W. Ding, and G. C. Schatz, J. Phys. Chem. C **122**, 29445 (2018).

[30] H. T. Dung, L. Knöll, and D.-G. Welsch, Phys. Rev. A **65**, 043813 (2002).

[31] J. Knoester and S. Mukamel, Phys. Rev. A **40**, 7065 (1989).

[32] G. Juzeliūnas and D. L. Andrews, Phys. Rev. B **49**, 8751 (1994).

[33] J. S. Ford, A. Salam, and G. A. Jones, J. Phys. Chem. Lett. **10**, 5654 (2019).

[34] D. Green, G. A. Jones, and A. Salam, J. Chem. Phys. **153**, 034111 (2020).

[35] M. C. Waller and R. Bennett, Phys. Rev. A **106**, 043107 (2022).

[36] A. Salam, Atoms **6**, 56 (2018).

[37] G. A. Jones and D. S. Bradshaw, Front. Phys. **7**, 100 (2019).

[38] D. P. Craig and T. Thirunamachandran, *Molecular Quantum Electrodynamics* (Dover, New York, 1998).

[39] A. Salam, *Molecular Quantum Electrodynamics: Long-Range Intermolecular Interactions* (Wiley, New York, 2009).

[40] A. Salam, WIREs Comput. Mol. Sci. **5**, 178 (2015).

[41] D. L. Andrews, G. A. Jones, A. Salam, and R. G. Woolley, J. Chem. Phys. **148**, 040901 (2018).

[42] D. L. Andrews, D. S. Bradshaw, K. A. Forbes, and A. Salam, J. Opt. Soc. Am. B **37**, 1153 (2020).

[43] D. P. Craig and T. Thirunamachandran, J. Chem. Phys. **109**, 1259 (1998).

[44] A. Salam, J. Chem. Phys. **122**, 044113 (2005).

[45] L. A. Nguyen, H. He, and C. Pham-Huy, Int. J. Biomed. Sci. **2**, 85 (2006).

[46] S. Bang, S. Y. Buhmann, and R. Bennett, arXiv:1912.05892.

[47] D. Kröner, J. Phys. Chem. A **115**, 14510 (2011).

[48] P. Horsch, G. Urbasch, K.-M. Weitzel, and D. Kröner, Phys. Chem. Chem. Phys. **13**, 2378 (2011).

[49] D. Kröner, Phys. Chem. Chem. Phys. **17**, 19643 (2015).

[50] C.-K. Duan, M. F. Reid, and Z. Wang, Phys. Lett. A **343**, 474 (2005).

[51] J. Fiedler, P. Thiyam, A. Kurumbail, F. A. Burger, M. Walter, C. Persson, I. Brevik, D. F. Parsons, M. Boström, and S. Y. Buhmann, J. Phys. Chem. A **121**, 9742 (2017).

[52] L. Onsager, J. Am. Chem. Soc. **58**, 1486 (1936).

[53] M. N. Polyanskiy, Refractive index database, https://refractiveindex.info (2022), accessed on 2022-07-08.

[54] W. Zhang, Q. Song, W. Zhu, Z. Shen, P. Chong, D. P. Tsai, C. Qiu, and A. Q. Liu, Adv. Phys.: X **3**, 1417055 (2018).